Iodide based electrochemical gold quantification method for lateral flow assays

Journal Article

Author(s):
Blickenstorfer, Yves; Jirasko, Vlastimil; Tanno, Alexander; Dräger, Sarah; Hoven, Darius; Löhle, Josephine; Leuch, Stephan; Mamedava, Yulya; Müller, Sereina Livia; Leuzinger, Karoline; Osthoff, Michael; Vörös, Janos (ID)

Iodide based electrochemical gold quantification method for lateral flow assays

Yves Blickenstorfer [a,b], Vlastimil Jirasko [a,b], Alexander Tanno [a,b], Sarah Dräger [c,d], Darius Hoven [a], Josephine Löhle [a,b], Stephan Leuch [a], Yulya Mamedava [b], Sereina Livia Müller [c,d], Karoline Leuzinger [e], Michael Osthoff [c,d], János Vörös [a,*]

[a] *Laboratory of Biosensors and Bioelectronics, Institute of Biomedical Engineering, ETH Zurich, Zurich, Switzerland*
[b] *Hemetron Ag, Thalwil, Switzerland*
[c] *Division of Internal Medicine, University Hospital Basel, Basel, Switzerland*
[d] *Department of Clinical Research, University Hospital Basel, University of Basel, Basel, Switzerland*
[e] *Clinical Virology, Laboratory Medicine, University Hospital Basel, Basel, Switzerland*

ABSTRACT

The lateral flow assay (LFA) is an ideal technology for at-home medical diagnostic tests due to its ease of use, cost-effectiveness, and rapid results. Despite these advantages, only few LFAs, such as the pregnancy and COVID-19 tests, have been translated from the laboratory to the homes of patients. To date, the medical applicability of LFAs is limited by the fact that they only provide yes/no answers unless combined with optical readers that are too expensive for at-home applications. Furthermore, LFAs are unable to compete with the state-of-the-art technologies in centralized laboratories in terms of detection limits. To address those shortcomings, we have developed an electrochemical readout procedure to enable quantitative and sensitive LFAs. This technique is based on a voltage-triggered *in-situ* dissolution of gold nanoparticles, the conventional label used to visualize target-specific signals on the test line in LFAs. Following the dissolution, the amount of gold is measured by electroplating onto an electrode and subsequent electrochemical quantification of the deposited gold. The measured current has a low noise, which achieves superior detection limits compared to optical techniques where background light scattering is limiting the readout performance. In addition, the hardware for the readout was developed to demonstrate translatability towards low-cost electronics.

1. Introduction

Almost forty years ago, the commercial introduction of the lateral flow assay (LFA) technology was a breakthrough for one of the most successful medical diagnostic home tests: the pregnancy test. Mak et al. (2016) The success of the pregnancy test has often overshadowed other diagnostic applications of LFAs including HIV Greenwald et al. (2006) or influenza. Peaper and Landry (2014) Similarly, applications in other fields, such as food testing or veterinary tests have remained a niche market in comparison to the pregnancy test. Wong and Tse (2009) However, in the COVID-19 pandemic, LFAs have received unprecedented attention due to the development of rapid SARS-CoV-2 antigen tests based on LFA platforms. The fast development and production of the rapid COVID-19 test was enabled by the technological maturity of LFAs including their ease of manufacturing and up-scaling. In addition, these assays are easy to use, low cost and give a quick result. Wong and Tse (2009) Therefore, LFA technology was ideal to serve the need of frequent and rapid testing and helped mitigating the spreading of SARS-CoV-2.

The LFA system consists of a strip with multiple zones of porous materials and is most commonly employed as a sandwich immunoassay (Fig. 1). The sample is applied to the test and capillary forces drive the liquid along the strip. The higher the target concentration, the more nanoparticles accumulate on the test line. Wong and Tse (2009) Despite their simplicity, LFAs are capable of generating rapid results at clinically relevant target concentrations. A major reason for this ability is the three-dimensional porous structure of the nitrocellulose. Biorecognition elements immobilized in this matrix provide short diffusion lengths for target analytes and nanoparticle labels assuring fast results. In addition, the large surface area of the nitrocellulose and the nanoparticles allows high density immobilization of biorecognition elements. The availability of many recognition sites shifts the equilibrium of target-to-receptor binding towards the bound state Hwu et al. (2020) allowing detection of lower target concentrations.

Despite the advantages of LFAs, they are still outperformed in sensitivity (limit of detection (LOD)) by assays commonly employed in
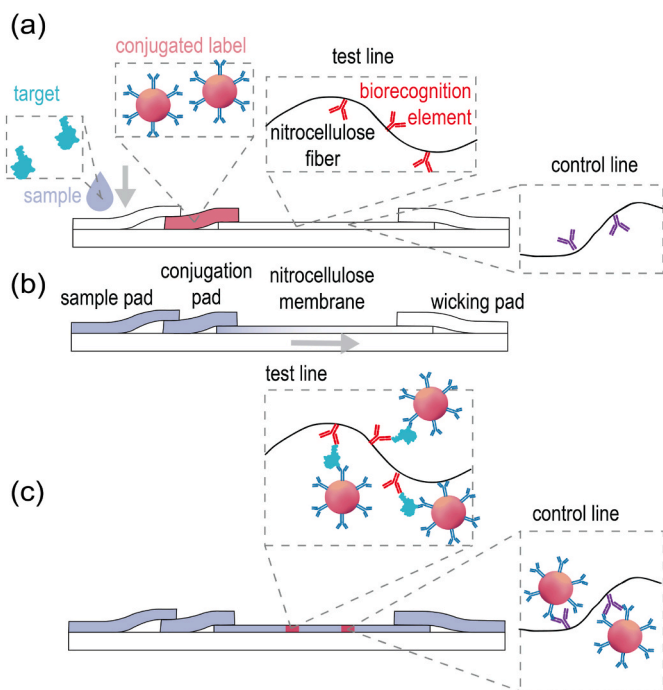

Fig. 1. Lateral flow sandwich assay (a) A sample is applied to the sample pad of a lateral flow strip. (b) The liquid flows through the conjugation pad and picks up gold nanoparticle labels. (c) An antibody-target-antibody sandwich causes the gold nanoparticles to accumulate on the test line indicating the target concentration. Direct antibody binding results in a control line, signaling a working assay.

centralized laboratories. To tackle this shortcoming, numerous strategies have been employed to improve the LOD of LFAs. One strategy tackles this challenge by modifying the nanoparticle labels. Mak et al. (2016) The state-of-the-art is using gold nanoparticles due to their visibly dark red color and ease of conjugation with bioreceptors of interest. Sometimes, colored latex particles are also used especially if multiplexing is desired, as different colors can be used for each target. Improved sensitivity may be achieved using alternative labels such as carbon nanoparticles or fluorescent quantum dots. Despite such interest in designing new labels, commercial LFAs are still mostly based on gold nanoparticles. Mak et al. (2016); Quesada-González and Merkoçi (2015); Ge et al. (2014).

Another limitation of LFAs is the interpretation by naked eye, which does not provide quantitative results. Diagnostic tests for pregnancies or infectious diseases only require a yes/no answer. Other applications such as assessing inflammation markers or the cardiac marker troponin require a quantitative result as these molecules are present in all patients and only the precise concentration indicates certain medical conditions. To this end, LFAs are combined with optical readers, which take an image of the strip and quantify the signal intensity of the test line. Urusov et al. (2019) This approach assures a quantitative result, but the expensive optics lead to reader costs that are typically above $1000. Yetisen et al. (2013) To enable quantitative tests without expensive readers, smartphone-assisted readout has received attention. Mak et al. (2016) A major issue of this approach is ensuring reproducible illumination, and correct timing of the readout requiring a camera-to-strip interface. Mudanyali et al. (2012) Such an interface has to be adapted and calibrated for each individual smartphone model hindering the applicability. Other solutions do not ensure reproducible illumination, which heavily reduces reproducibility. Therefore, these tests are mostly used to provide qualitative results. The digital yes/no displayed on the screen avoids possible misinterpretation of the result by an untrained user. Urusov et al. (2019); Vashist et al. (2014) Another qualitative approach to enable easier interpretation of the results are cost-efficient,

photodiode-based readers displaying a digital result on a low-cost screen. Robinson et al. (2007) For medical applications, this technology facilitates regulatory clearance compared to smartphone-based readout, by avoiding the issue of differences in the variety of smartphone models.

To overcome the aforementioned shortcomings of optical detection and combine a low-cost reader with enhanced sensitivity, alternative readout mechanisms have been explored. Inspired by the cost-effective glucometers, electrochemical detection methods are applied to paper membranes Mazurkiewicz et al. (2020) and for LFAs in particular. Nie et al. (2010) A promising electrochemical readout based on the quantification of the metal ions contained in the assay label Dequaire et al. (2000); Wang et al. (2001) has been applied to LFAs. Liu et al. (2014) The material of the labels include Bi^{3+}, Lu et al. (2005) quantum dots, Liu et al. (2007, 2008); Nian et al. (2012) or gold nanoparticles. Mao et al. (2008); Ivandini et al. (2015) Upon completion of the assay, a strong acid, such as hydrogen bromide (HBr), is added to release metal ions from the labels. Next, the ions are quantified by anodic stripping voltammetry. A cathodic voltage is applied to an electrode, which causes the ions to be electroplated onto the electrode. Finally, the voltage is increased to an anodic potential, which causes the plated metal to oxidize and strip from the electrode. The released electrons cause a measurable signal proportional to the initial amount of the label. This technique enables a quantitative readout that is more sensitive than conventional optical detection and can be implemented by a cost-effective potentiostat. Liu et al. (2014) In addition, this method is compatible with gold nanoparticle labels. However, the reported methods require the manual addition of a strong acid, which is not feasible outside of a laboratory. Further, the biochemical assay must be completed before the manual addition of the acid. Therefore, a user must wait for the duration of the assay and perform an additional user step at a precise time point, which reduces the user-friendliness of the approach.

We overcame the requirement of manually adding toxic chemicals for ion release by electrochemical *in-situ* dissolution of gold nanoparticle labels. The *in-situ* dissolution can be triggered automatically at a precise time point without any additional user steps. The dissolution is based on harmless iodide chemistry, which is compatible for use outside of laboratories. Iodide chemistry could previously not be used for gold quantification in LFAs due to an overlap of the redox potentials with gold oxidation causing a background current. The use of the chemistry in this manuscript is enabled by the choice of the working electrode material, indium tin oxide (ITO). In contrast to other electrode materials such as screen printed carbon, we demonstrate that ITO shows minimal interference reactions with the dissolution chemistry at the critical potentials allowing for low background currents. This property is key for achieving good LODs. To the best of our knowledge, this characteristic feature of ITO has not been demonstrated before. The LOD for the detection of gold nanoparticles is improved by more than two orders of magnitude compared to optical quantification of LFAs. Integration into a real world system is demonstrated in a COVID-19 assay. The LOD for this assay detecting the nucleocapsid protein is at 840 fM. The clinical performance was verified by testing 194 patient samples achieving a diagnostic sensitivity of 92.1 % and a diagnostic specificity of 96.8 % compared to the gold standard reverse transcription polymerase chain reaction (RT-PCR). A better performance is currently hindered by the non-specific adherence of the gold nanoparticles to the nitrocellulose. Further optimizations in membrane and nanoparticle treatment would enable exploitation of the full potential of the electrochemical methodology for highly sensitive at-home medical tests. Such electrochemical LFAs have the potential to translate diagnostic tests that are currently only performed in centralized laboratories, directly to patient homes.

2. Methods

2.1. Electrodes and cassettes

Disposable working electrodes were manufactured by cutting cost-effective indium tin oxide deposited on polyethylene terephthalate (Diamond Coating) into 2 mm × 18 mm sized rectangles with a Cameo 4 plotter (Silhouette). To be compatible with mass manufacturing, the reference and counter electrodes consisted of screen printed carbon (Henkel, EDAG PF 407C E&C) on polyethylene terephthalate foil (MDV, Robuskin PET). After screen printing through a 80 T mesh (Siebdruckversand) with a 80 shore squeegee (Siebdruckversand), the ink was dried for 30 min at 90 °C and cut into 1 mm wide pieces (reference electrode) and 2 mm wide pieces (counter electrode) using the Cameo 4 plotter. Plastic cassettes were manufactured to hold the electrodes and strips at the correct location. The cassettes were 3D-printed with a liquid crystal display resin printer (Phrozen, Sonic Mini 4K) using the corresponding resin (Phrozen, Aqua Resin Grey 4K). One working electrode, one reference electrode, and two counter electrodes were assembled into each cassette manually.

2.2. Quantification of dispensed gold nanoparticles

A nitrocellulose membrane (Cytiva, FF80HP Plus Thick) was manually placed onto a backing card (DCN, MIBA-020). An empty conjugation pad (Cytiva, Whatman Standard 14) was cut into 5 mm width and placed at the lower end of the nitrocellulose membrane with an overlap of 2 mm. Bare gold nanoparticles (Cytodiagnostics, G-40-20-10) were diluted in water to reach the desired concentration. A line of gold nanoparticles was dispensed on the nitrocellulose membrane with a self-built dispenser at 50 nl/mm in contact mode. A crepla sheet of 14 mm was glued on the backside of the backing cards. The assembled cards were cut into 4 mm wide strips. The strips were placed with the empty conjugation pad into 96-well plate with 40 μl testing buffer (Hemetron) containing I^- ions. After a strip was fully wetted, it was either assembled into a cassette containing the electrodes, or used for optical quantification. For optical quantification the strips were placed next to each other to ensure uniform illumination. Next, the strips were photographed from a distance of 35 cm using a digital camera (Canon, EOD 6D) which had a 100 mm macro lens. The image was taken without exposure correction and the settings consisted of an aperture of 7.1, a shutter speed of 1/125 s, and an ISO value of 640. Illumination was performed with an LED ring flashlight (Emiral) mounted on the camera via top shoe connector for synchronization at +1.5 flash strength. The images were analyzed in Fiji. Schindelin et al. (2012) For each strip, an analysis region was defined by a rectangle slightly narrower than the strip itself to avoid interference effects at the edges. An intensity profile of the rectangle was collected in the flow direction of the strip, averaging all pixels perpendicular to the flow direction. A linear fit was used to compensate for illumination gradients and the background was subtracted. The maximum absorbance was determined around the expected location of the line. For the electrochemical quantification, the electrodes were brought in contact with a potentiostat (Metrohm, Autolab PGSTAT302N). A current scan from 0 to 0.16 mA was applied to convert I^- to I_3^- causing gold dissolution that resulted in the formation of AuI_2^- complex ions. Next, the dissolved gold was plated for 120 s at an applied voltage of −1.2 V. Finally, a linear voltage scan (0.1 V/s) was applied from −1.2 V to 1.2 V and the measured current was used to quantify the target in the sample. To compare the electrochemical measurement to the optical data, both signals were normalized with the formula: $y_{i,\text{norm}} = \frac{y_i - \min y}{\max y - \min y}$, where y represents the optical and electrochemical signals, respectively.

2.3. Preparation of the LFA strips for detection of the SARS-CoV-2 nucleocapsid protein

Gold nanoparticles (10 optical density (OD)) (Cytodiagnostics, G-50-20) conjugated to rabbit monoclonal antibody (Hytest, 3CV4 C706) against SARS-CoV-2 nucleocapsid mixed with dispensing drying buffer (20% sucrose, 10% trehalose, 2% BSA, 5 mM Tris pH 7.5) in a ratio 1:1 were dispensed on the conjugation pad material (Cytiva, Whatman Standard 14) with a self-built dispenser at a volume of 2.5 nl/mm in contact mode dispensing. The conjugation pad was then cut to 5 mm wide strips. The nitrocellulose membrane (Cytiva, FF80 HP Plus Thick) was manually placed onto a backing card (DCN, MIBA-020). The rabbit monoclonal antibody against SARS-CoV-2 nucleocapsid (2.5 mg/ml) for the test line (Hytest, 3CV4 C715) and a goat anti-rabbit polyclonal antibody (2.5 mg/ml) for the control line (Invitrogen, A16098) were dispensed at 50 nl/mm using a self-built dispenser in contact mode, dispensing 9 mm and 19 mm from the upstream edge of nitrocellulose membrane, respectively. The 5 mm strip of conjugation pad was placed on the top of the upstream edge of nitrocellulose with 1.5 mm overlap. The sample pad (Millipore, CFSP) and the wicking pad (Millipore, CFSP) were manually placed on the top of the conjugation pad and the nitrocellulose membrane with respectively 1.5 mm and 3 mm overlaps. The cards were then cut into 4 mm wide strips with a common guillotine paper cutter (Dahle). The strips were placed into the cassettes and stored until used either in a vacuum desiccator or packaged with a vacuum sealer (Cecotec, SealVac). For the clinical evaluation the tests were stored between two and three months.

2.4. COVID-19 assay quantification

Saliva was collected from different apparently healthy donors with buccal swabs (COPAN, FLOQSwabs). All donors gave their consent and the saliva was anonymized. The swabs were immersed in a disposable plastic microcentrifuge tube containing 1.2 ml of viral transport medium, 0.86x Hanks balanced salt solution (Gibco 14060040) adjusted to pH 7.4 with sodium bicarbonate, and rotated 10 times. The samples were frozen until they were used. After thawing, recombinantly expressed and purified nucleocapsid protein (Biorbyt, orb638744) was added to reach the described concentration. Next, concentrated running buffer (Hemetron) was added in a ratio of 1:4.8. 70 μl of this mixture was added to the cassette opening followed by 70 μl of the rinsing buffer (Hemetron). The assay was run for 20 min. The assay was run identically for the optical readout as for the electrochemical readout.

The optical and electrochemical readout started after the assay had finished. The wet strips were removed from the cassettes (full assay) and placed next to each other to ensure uniform illumination. Next, the strips were both photographed (Canon, EOD 6D) and analyzed (Fiji) as described in the section on the quantification of the dispensed gold nanoparticles. For electrochemical quantification, the cassettes containing the strips (supporting information Fig. S1a) were inserted into a holder (supporting information Fig. S1b) which cut the nitrocellulose in the proximity of both pads to avoid any further capillary driven flow. This holder ensured good contact between electrodes and strips by applying a small mechanical force on the strip. The holder also ensured good contact between the electrodes and the spring contacts (PTR Hartmann, 1015-D-1.5N-AU-0.75) which were connected to a custom-built potentiostat. A linear potential scan up to 1.2 V was applied to convert I^- to I_3^- and caused gold dissolution forming an AuI_2^- complex ion. Next, the dissolved gold was plated for 120 s at an applied voltage of −1.2 V. Finally, a linear voltage scan (0.1 V/s) was applied from −1.2 V to 1.2 V and the measured current was used to quantify the target in the sample. The measured current was smoothed with a rolling average with a window size of 30 data points. Next, a linear fit of the current between 0.2 V and 0.55 V was made while restricting both the slope and the offset, to under 0.5 μA. The fitted line was subtracted from the measured current and a peak finding algorithm was applied to identify the peak

current of each curve. If no peak was found, the maximal current value between 0.35 V and 0.4 V was taken. To compare the electrochemical measurement to the optical data, the signal was normalized with the formula: $y_{i,norm} = \frac{y_i - \min y}{\max y - \min y}$, where y represents the optical and electrochemical signals, respectively.

2.5. Clinical procedure

The prospective observational study was conducted in accordance with the protocol, the Declaration of Helsinki, the principles of Good Clinical Practice, the Human Research Act (HRA), and the Human Research Ordinance (HRO). It was approved by the Ethics Committee of Northwest and Central Switzerland (EKNZ project ID, 2020–02260). Adult patients enrolled in the study, who signed informed consent, had suspicion of SARS-CoV-2 infection with symptom onset within the previous 10 days and either confirmed SARS-CoV-2 infection or were SARS-CoV-2 negative with or without detection of another virus causing respiratory tract infections. A nasopharyngeal and a pharyngeal swab was collected in all participants by a trained healthcare worker. After the collection, the two swabs were pooled and placed into a tube containing viral transport medium and labelled with a unique study number in a way that the participants cannot be identified. The samples were transported to the clinical laboratory within 2 h after collection. Subsequently, the samples were aliquoted and either immediately analyzed by reverse transcription quantitative PCR targeting the S-gene of SARS-CoV-2 as a reference method for determining RNA load Leuzinger et al. (2021) or frozen at −80 °C until analysis with the electrochemical rapid antigen tests.

3. Results

To enable cost-effective and sensitive readout of LFAs, gold nanoparticle labels were quantified electrochemically. First, the nanoparticles were dissolved by an *in-situ* generated dissolution chemistry. Subsequently, the resulting gold ions were electroplated on an electrode and quantified by anodic stripping voltammetry. The sensitivity of electrochemical detection was compared to optical detection using dispensed lines of gold nanoparticles on nitrocellulose, as well as in a real assay, i.e. a COVID-19 antigen rapid test. Finally, translatability to the real world is demonstrated by measuring clinical patient samples with the electrochemical COVID-19 antigen rapid test.

3.1. Electrochemical procedure

The first step after completion of the assay is the dissolution of the gold nanoparticles in the three-dimensional matrix below the electrode. To this end, potassium iodide (KI) is introduced to the system with the rinsing buffer at the beginning of the assay. The dissolution is initiated electrochemically only after the assay has been completed. The indium tin oxide working electrode is located above the test line (Fig. 2a). The dissolution is initiated either by applying a positive current or a voltage scan to the indium tin oxide working electrode (Fig. 2b). Qi and Hiskey (1993).

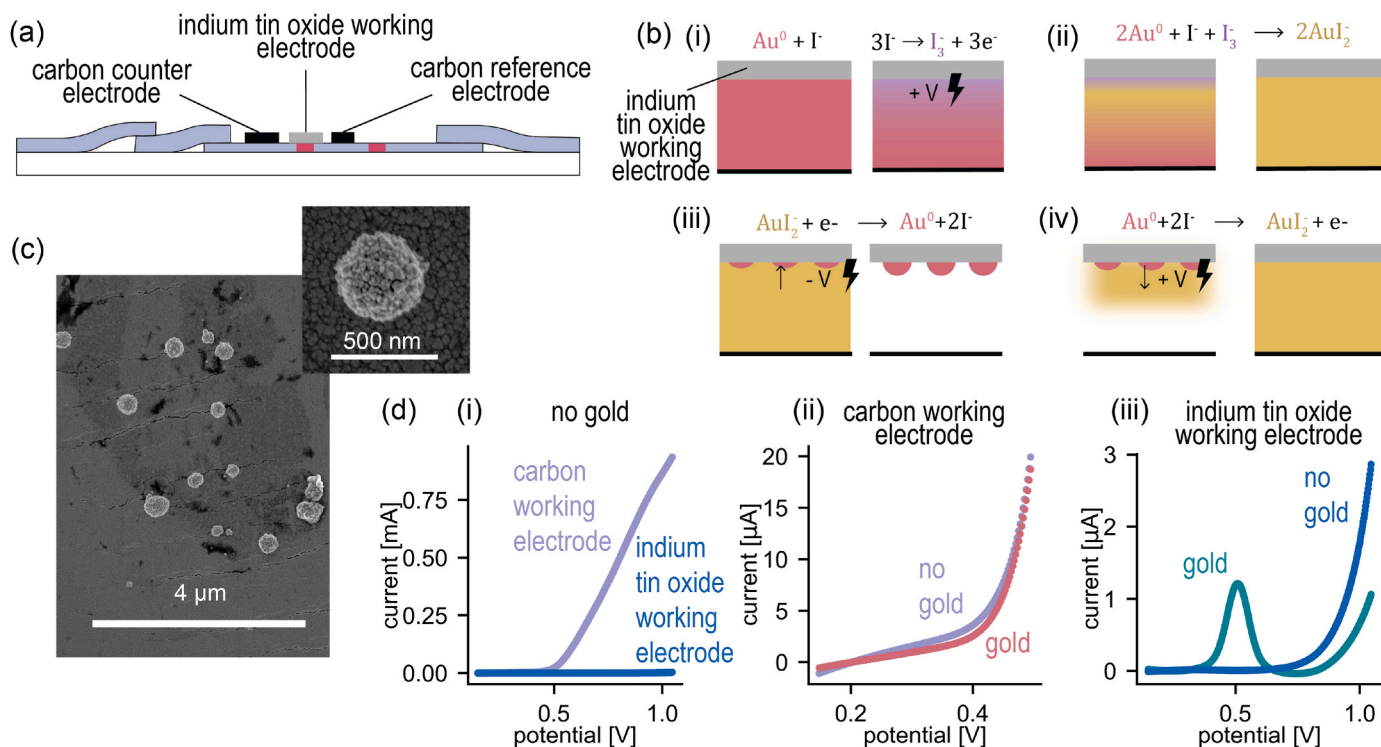$$3I^- \rightarrow I_3^- + 3e^- \qquad E^\circ = 0.525 \ V \qquad (1)$$

Fig. 2. (a) A counter electrode (carbon), a working electrode (indium tin oxide), and a reference electrode are in contact with the strip. (b) The electrochemical procedure starts after the test line has formed. (i) Upon application of an anodic potential iodide (I^-) is oxidized to triiodide (I_3^-) on the indium tin oxide electrode. (ii) The mixture diffuses in the bulk and causes gold dissolution. (iii) The gold ions diffuse to the electrode surface where they are electroplated onto the indium tin oxide at a cathodic potential. (iv) The amount of plated gold is quantified upon a potential scan from a cathodic to anodic potential. At the anodic potential, the gold is oxidized and stripped form the electrode causing a current. (c) Scanning electron microscopy images of electroplated gold on the indium tin oxide electrode. (d) Current measurement during potential scans after the electroplating shows the importance of the working electrode material. (i) Without any gold in the system the carbon working electrode shows the expected increasing current above 0.5 V due to the iodide oxidation reaction. On indium tin oxide the slow electron transfer rate for the iodide oxidation results in a background current orders of magnitude smaller than for a carbon working electrode. (ii) The large background current on the carbon working electrode obstructs the measurement of the gold oxidation. (iii) On indium tin oxide working electrodes, the low background currents reveal the oxidation peak of the deposited gold.

The standard electrode potential E° is given with respect to the standard hydrogen electrode. Applying an overpotential to the working electrode causes the production of I_3^- while electrons are flowing into the electrode, generating a measurable current.

Mixtures of I^-/I_3^- effectively dissolve gold. The mixture diffuses into the nitrocellulose below the electrode and dissolves the gold nanoparticles spontaneously forming diiodoaurate AuI_2^-.

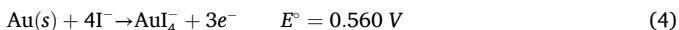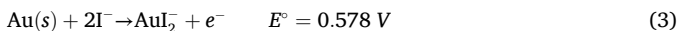$$2Au(s) + I^- + I_3^- \rightarrow 2AuI_2^- \tag{2}$$

The non-toxic nature of iodide mixtures makes it a common choice for gold dissolution in microfabrication. Davis and Tran (1991); Green (2014).

In the next step, a cathodic potential is applied to the working electrode. The diiodoaurate diffuses to the electrode where it is reduced to solid gold. The reduction causes a current (Fig. 2biii). However, the plating current is not suitable for the quantification of the gold. As each gold iodide complex ion needs to diffuse to the electrode, plating currents are low in value. In addition, when switching from dissolution to plating potentials, the sudden voltage change of more than 2 V induces a large capacitive current that initially masks any faradaic currents stemming from electrochemical reactions. Furthermore, the high cathodic plating potential results in competing faradaic currents larger than the current caused by the electrodeposition of gold, obstructing quantification during the plating process. To verify the gold plating, scanning electron microscopy (SEM) of the indium tin oxide working electrode was conducted (Fig. 2c). It is apparent that the plating does not result in a homogeneous film but rather in spherical gold islands.

The electrochemical dissolution offers significant advantages over manually adding a strong acid such as HBr. While HBr is highly corrosive and irritating to inhale, KI is harmless and even used in food supplements. For applications outside of the laboratory, a non-hazardous chemistry is needed. Because KI itself does not dissolve gold, it can be added with the rinsing buffer at the beginning of the assay. Therefore electrochemical dissolution is much more user-friendly than chemical dissolution where the chemistry has to be applied at the end of the assays to the right location. This is especially critical when developing a diagnostic test that should be used in a home environment. Finally, the location of the dissolution is defined by the electrode. The diffusion of I_3^- is confined at the electrode over the period of a measurement. Therefore, only gold nanoparticles at the right location are dissolved and contribute to the signal.

After the dissolution and electroplating of gold nanoparticles, the quantification is performed. The potential on the indium tin oxide working electrode is scanned linearly from the cathodic plating potential to an anodic potential. As the voltage reaches anodic potentials, the plated gold is oxidized and stripped from the electrode. Qi and Hiskey (1993).

$$Au(s) + 2I^- \rightarrow AuI_2^- + e^- \qquad E° = 0.578 \, V \tag{3}$$

$$Au(s) + 4I^- \rightarrow AuI_4^- + 3e^- \qquad E° = 0.560 \, V \tag{4}$$

The gold oxidation results in gold stripping from the electrode causing a current peak. The distinctiveness of this peak (e.g. its height or area) is proportional to the initial amount of gold nanoparticles.

The standard electrode potentials of the gold stripping reactions are only slightly higher than the standard electrode potential of the I^- to I_3^- oxidation. This fact can provide a severe obstacle for the procedure when employing commonly used working electrode materials such as carbon. During the measurement, the potential is scanned from a cathodic to an anodic potential. When reaching the potential at which the gold is stripped, the I^- is oxidized to I_3^- simultaneously on most working electrode materials causing a large background current. Due to orders of magnitude higher concentration of I^- compared to gold, this background current obstructs any quantification of the gold peak.

Fig. 2d shows how the large background current on a carbon working

electrode hinders the detection of a gold stripping peak. When changing the working electrode material to indium tin oxide, the background current is orders of magnitude smaller. Indium tin oxides has a small electron transfer rate for I^- oxidation. Therefore, the standard electrochemical rate constant is lower compared to carbon causing a smaller background current at potentials relevant for gold detection. This property of the working electrode results in a large enough potential window to detect the gold oxidation peak which is necessary for a sensitive detection of gold.

While the electrochemical method requires additional materials compared to an optical test, the small area of the electrodes results in a negligible contribution to the costs of a test. The ITO electrode costs are well below one cent per test and the carbon electrodes represent even lower costs. Similarly, the iodide cost is below one cent per test. The placement of the electrodes in the cassettes represents an additional step in the manufacturing. While automatized pick and place methodologies for this task exist, the step requires careful consideration for large-scale manufacturing.

3.2. Electrochemical nanoparticle detection

The sensitivity of the electrochemical readout methodology was demonstrated by measuring different concentration of bare gold nanoparticles, dispensed as lines on nitrocellulose (Fig. 3). The gold nanoparticle concentration is described with the unit optical density (OD). For the 40 nm gold nanoparticles used herein, 1 OD corresponds to approximately 14 million gold nanoparticles per line of each strip. The optical density scales linearly with the gold nanoparticle concentration. The concentration of gold nanoparticles varied over four orders of magnitude. The LOD is defined as the concentration at which the linear fit of the data reaches the value of the signal at zero analyte plus three times standard deviation at zero analyte concentration. The currents measured during the voltage scan resulted in a gold oxidation peak. Larger gold concentrations resulted in larger oxidation peaks (Fig. 3a and b).

For comparison, the strips have been analyzed optically by eye and with a high-end camera (Fig. 3c and d). By eye, 1 OD represents a faint line while 0.3 OD is not visible. The camera images are analyzed by their intensity profile where a deposited line presents itself as a dip in intensity.

The direct comparison between electrochemical signal (oxidation peak height) and the optical signal (absorption) is visible in the dose response curve depicted linearly (Fig. 3e) and double logarithmically (Fig. 3f). The optical and electrochemical readout show a linear response over the measured range. Only at the largest gold concentrations, some saturation is visible for the electrochemical method. The error of the electrochemical method scales with the amount of gold, i.e., it is high at large signals and lower at smaller signals. In contrast, the error of the optical method is more constant. A reason for this behavior is the contribution of the scattering of the paper to the signal. This aspect renders the electrochemical method more appropriate for smaller signals. Consequently, electrochemical detection is more adept for direct assays than for competitive assays.

The approximate electrochemical LOD is at 0.0018 OD or about 21′000 gold nanoparticles. For the optical analysis evaluating the intensity of the camera image resulted in a LOD of approximately 0.29 OD corresponding to 4.1 million nanoparticles which is slightly better than analysis by eye. As such, the electrochemical readout improves LOD of the gold nanoparticle detection by over two orders of magnitude compared to the optical readout (Fig. 3f). This improvement is primarily due to the following factors:

· For the optical method, the detected light increases for lower analyte concentrations. The noise of this background signal is large in the absence of any analyte. In contrast, for electrochemical detection,
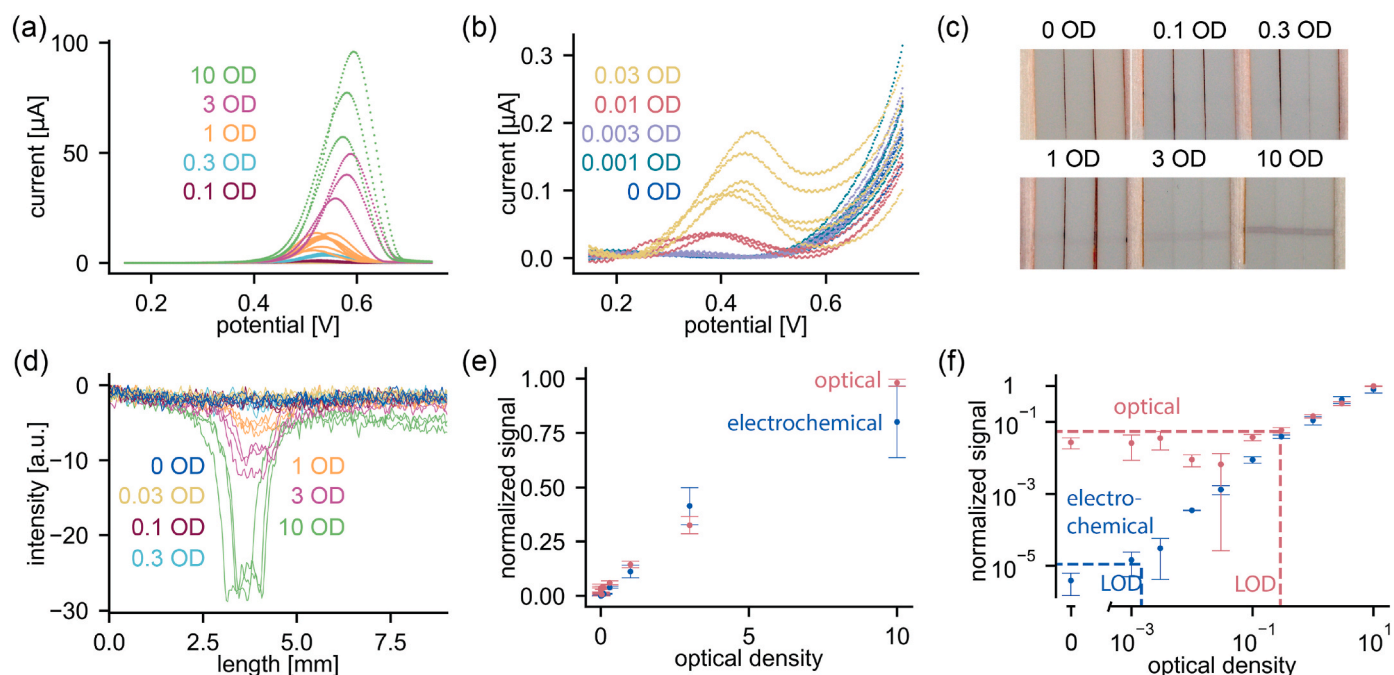
Fig. 3. Gold nanoparticles were dispensed as lines on nitrocellulose at different concentrations for electrochemical and optical quantification (1 OD = 14 million gold nanoparticles) (a) Current measurements of the electrochemical detection method show larger gold oxidation current peaks for larger gold concentrations. (b) Current measurements of the electrochemical detection method at low gold concentrations show small oxidation peaks. (c) Image of strips with lines of dispensed gold nanoparticles taken with a high-end optical camera. Similar to the camera image, the naked eye can detect 1 OD as a faint line. (d) Intensity cross section averaged over the strip width for different gold concentrations. The dispensed peak can be optically detected as a dip in intensity (e) Dose response curves of the electrochemical and optical detection show a linear response of signal to amount of dispensed gold (Pearson correlation coefficients: electrochemical readout 0.9797, optical readout 0.9991) (f) Double logarithmically scaled dose response curve of the electrochemical and optical detection reveals that the limit of detection is approximately 2 orders of magnitude better for the electrochemical method (0.0014 OD) than for optical detection (0.29 OD). For the LOD determination the following fitting equations were used: electrochemical readout $0.045x - 0.0000551$, optical readout $0.096x + 0.026$ (supporting information Figure S2).

the current decreases for lower analyte concentration. The noise of the background is lowest in the absence of analyte.

· The low background currents are enabled by the slow electron transfer rate of the indium tin oxide electrode for iodide oxidation.
· While the optical readout only detects the gold nanoparticles in the top 10 μm of the LFA, all captured nanoparticles are dissolved and accumulated for the electrochemical analysis.

3.3. Analytical performance of a SARS-CoV-2 assay

To apply the readout methodology to a relevant system, we have developed an LFA for detecting SARS-CoV-2. The LFA strip captured the target nucleocapsid protein along with a secondary antibody-coated gold nanoparticle on a test line. Eleven buccal swab samples of apparently healthy anonymized donors were collected in a viral transport medium. Nucleocapsid protein was added at different concentrations before running the test. The resulting signal was analyzed optically and electrochemically.

Most diagnostic tests for COVID-19 rely on samples collected with nasopharyngeal swabbing. Alternatively, buccal swabbing can be used in some diagnostic tests for COVID-19. Blanco et al. (2022) This procedure is easier to perform for untrained patients and more comfortable in comparison to the commonly used nasopharyngeal swabbing. Samples from both nasopharyngeal swabbing and buccal swabbing show considerable variations between patients including differences in viscosity and the concentrations of proteins and other biomolecules. In addition, buccal swab samples show variations due to contamination and pH altering caused by food intake. Thus, buccal swabbing is an attractive method but results in a challenging matrix for biosensing. Miočević et al. (2017) Since COVID-19 tests only require a yes/no answer, the variations stemming from the matrix are less of an issue than
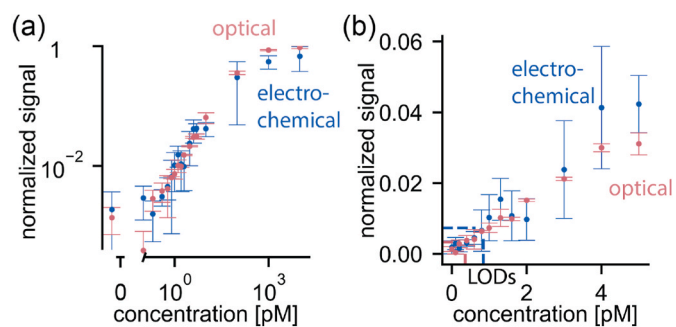
for a test which requires quantitative results.

Fig. 4. Optical and electrochemical dose response of a full assay for the SARS-CoV-2 nucleocapsid protein spiked into buccal swab samples. (a) Logarithmic scaling demonstrates the dynamic range of both assays. The signal saturates at higher concentration but no drop due to a hook effect was observed yet. In contrast to the measurements on dispensed gold lines (Fig. 3), the detection limit is not improved by the electrochemical method. Background signal stemming from gold bound non-specifically to the nitrocellulose membrane obstructs detection at lower concentrations. (b) The linear representation at small concentrations shows how the variations are larger for the electrochemical method than for optical detection because the electrochemical method is effected more by variations of the buccal swab samples. Each concentration was measured in buccal swabs from multiple anonymized donors (n = 3–7). In total 11 buccal swab samples of apparently healthy donors were used for the electrochemical measurements. The LODs are 0.8 pM for electrochemical readout and 0.4 pM for optical readout. For the LOD determination the following fitting equations (in pM) were used: electrochemical readout $0.00867x + 0.000068$, optical readout $0.00655x + 0.00099$ (supporting information Figure S3).

The optical dose response illustrates a LOD of 0.4 pM (Fig. 4a and b). An LOD of 0.4 pM is better than most SARS-CoV-2 LFAs reported in the literature. Even SARS-CoV-2 antigen tests evaluated with high-end optical readers show values above 1 pM. Liu et al. (2022); Corman et al. (2021); Szekely et al. (2022); Bourassa et al. (2021) A reason for the low LOD of our test is the high affinity antibody which was dispensed at high concentration. In addition all strips have been imaged on a single high quality picture minimizing variations in illumination. Our assay shows an increasing signal until 1 nM nucleocapsid protein concentration and saturates at 10 nM (Fig. 4a). The concentration of our nucleocapsid stock solution limited the collection of data at higher concentrations at which a signal decrease is expected due to the hook effect: The target nucleocapsid protein saturates the antibodies on the gold nanoparticles and the antibodies on the membrane obstructing the formation of a sandwich. Wong and Tse (2009); Hwu et al. (2020) This effect limits the quantitative dynamic range to about three orders of magnitude. However, even if the signal decreases at larger values positive/negative diagnosis is possible as long as a signal is generated. This is important as the viral load may vary enormously between patients.

The electrochemical analysis of the assay resulted in a comparable LOD of 0.8 pM (Fig. 4a and b). As mentioned above, this LOD is competitive with commercially available rapid antigen tests. However, in contrast to our experiments with dispensed gold nanoparticles (Fig. 3), the electrochemical LOD of the assay is not better than the optical method. A better electrochemical LOD is hindered by non-specific binding. Even small amounts of gold nanoparticles non-specifically binding to nitrocellulose at zero target concentration caused a significant background signal due to the highly sensitive electrochemical transducer. Compared to the optical readout, the electrochemical signal was affected more by non-specific background because the electrode area was significantly bigger than the area of the test line. The size mismatch caused gold detection in a larger area than the test line, leading to higher background signals. The reason for the large electrode area was to ensure alignment of the test line and electrode in the manual assembly. The method for dispensing of the antibodies described in this manuscript did not allow for a perfectly reproducible positioning of the test line. A precise test line position enabled by state-of-the-art industrial manufacturing will improve the electrode alignment allowing for smaller measurement electrodes. We expect that the electrode width can be reduced by 60–80 % reducing the contribution of background signal and improving the LOD. The components for lateral flow assays, such as nitrocellulose membrane, gold particles, and assay buffer components have been optimized for optical detection over four decades leading to assays where the non-specific binding of the gold particles is just below the optical detection limit. To translate the ability of the electrochemical method to detect smaller amounts of gold particles to better assay LODs requires improvements of the lateral flow assay components to further reduce the non-specific binding. For example, improved passivation of the membrane and particles or improved rinsing ability of the assay could be explored.

Another aspect limiting the performance of the electrochemical quantification in the full assay was the increased noise compared to detecting dispensed gold particles. The increased noise is mostly due to the variation of saliva from different donors which affects the electrochemical readout more than the optical detection. The biomolecules present in the buccal swab samples interact with the iodide system Ayranci and Duman (2004); Ramachandran (1956) and dissolved gold. Glišić et al. (2012) Buccal swabbing results in variable concentration of interfering molecules between different donors, increasing the variations in the electrochemical signal. In addition, differences in saliva viscosity effect the running through the LFA further increasing the variations between donors (supporting information Fig. S4).

Another potential source of noise are the different electronic readout devices used for dispensed gold nanoparticles *versus* the full assay. The full assay was quantified with ten custom-built, Arduino-controlled potentiostats (supporting information Figs. S5, S6, and S7) instead of the one high-end potentiostat used for measuring the dispensed gold nanoparticles. Measuring with these ten devices enabled rapid parallelized measurements and demonstrated the feasibility of transitioning into low-cost electronics. An analysis of the device costs is given in the supporting information including a detailed list with the prices for each component in Table S1. While the average signal was similar for both readout devices, the electrical noise of the Arduino system was larger resulting in variations at low currents (supporting information Fig. S5). Further development and standardization of the readout electronics is needed to improve the measurements.

3.4. Clinical performance of a SARS-CoV-2 rapid test

Electrochemical SARS-CoV-2 rapid tests were deployed at the University Hospital Basel in a clinical setting to measure 194 patient samples: 101 SARS-CoV-2-positive patients, 78 SARS-CoV-2-negative patients and 15 SARS-CoV-2-negative patients positive for a respiratory virus other than SARS-CoV-2. These measurements demonstrate the user-friendliness of the electrochemical procedure and illustrate that the test can be translated to a real world setting. The translatability towards low-cost electronics were demonstrated by using three custom-built potentiostats (supporting information Figs. S5, S6, and S7) allowing for parallelized measurements. The 194 tests were performed by healthcare professionals. Further, the clinical setting demonstrated how a significant number of tests could be manufactured, shipped, and stored, illustrating scalability.

The clinical samples were quantified with the electrochemical rapid tests and with the reference quantitative PCR. In contrast to the analytical test where recombinant nucleocapsid protein was spiked into buccal swab samples, the clinical samples were collected by a nasopharyngeal/pharyngeal swab. This sample collection method is standard in the local clinical setting for quantification with PCR.

The direct comparison of the RNA load (in copies/ml) quantified by PCR and the result of the electrochemical rapid test is shown in Fig. 5a. The determination of test efficiency involves defining a threshold, as indicated by the horizontal line. Values above the threshold represent positive tests, values below the line represent negative test. To determine the threshold a receiver operating characteristic (ROC) curve is shown in Fig. 5b. Each data point represents a virtual threshold from which the true positives (diagnostic sensitivity) and false positives (1 - diagnostic specificity) are evaluated. The optimal trade-off, identified in the top left corner, achieved a diagnostic sensitivity of 92.1 % and a diagnostic specificity of 96.8 % with the measured patient samples. These values compare to commercial gold standard COVID-19 rapid
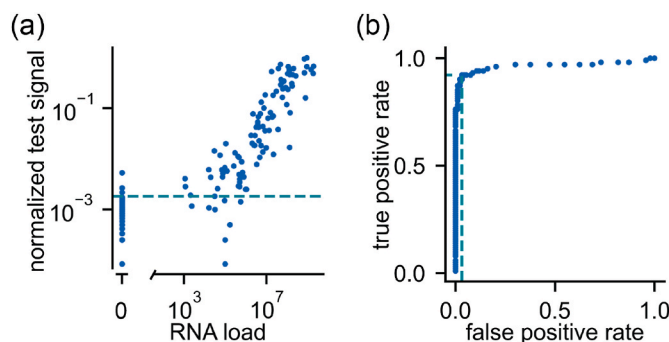
Fig. 5. Clinical performance of the electrochemical rapid test. (a) Electrochemical test result of 194 patient samples plotted against the viral load which was determined with RT-PCR. The horizontal line indicates the positive/negative threshold. (b) Receiver operating characteristic (ROC) curve: Each point represents a different threshold assessing if a test is positive. The curve depicts true positives (diagnostic sensitivity) on the y-axis and false positives (1 - diagnostic specificity) on the x-axis. The curve illustrates how a diagnostic sensitivity of 92.1 % and a diagnostic specificity of 96.8 % could be achieved.

antigen test results reported in literature Leber et al. (2021); Hogg et al. (2023); Khalid et al. (2022) although direct comparison is challenging due to differences in the clinical study. For example, the disease state of the patient cohort effects the viral load of the patients. Puhach et al. (2023).

Similar to the analytical evaluation, the test performance is limited by the non-specific binding of gold particles to the nitrocellulose membrane. Nevertheless, the clinical evaluation demonstrated how the electrochemical rapid antigen test can be transferred to a real world environment.

4. Conclusions

Electrochemistry offers a cost-effective alternative to expensive optical readers for the quantitative readout of LFAs. The method based on iodide/iodine chemistry dissolves the gold nanoparticle labels *in-situ* without harmful chemicals. The electrode material, indium tin oxide, allows an electrochemical readout with an improved LOD for the detection of gold nanoparticles by more than two orders of magnitude compared to the optical readout. Combining the readout with LFAs resulted in a sensitive SARS-CoV-2 rapid test comparable to commercial optical rapid tests. Finally, deploying the test in clinical setting where 194 patients samples were measured by healthcare professionals demonstrated user-friendliness of the test and resulted in a diagnostic sensitivity of 92.1 % and a diagnostic specificity of 96.8 %. A better performance was obstructed by the non-specific binding of the gold nanoparticles to the nitrocellulose membrane. To date, these membranes have been solely optimized for optical detection of the gold nanoparticles. The improved sensitivity of the electrochemical readout now requires further optimization of these membranes to reduce non-specific binding causing high background signals. Further, the background could be minimized by optimizing nanoparticle coatings or running buffers. In addition, controlled pretreatment of the electrodes will increase reproducibility. Automating the manufacturing could further improve the performance allowing for better alignment of smaller electrodes causing less background. The electrochemical readout method can detect any analyte that can be implemented in a direct lateral flow assay format. In addition, it is compatible to other matrices including blood. Therefore, we hope that the method will be applied in other assays to explore its potential for improving LFA sensitivity and detection ranges of various analytes. The inherently quantitative response, the low LOD, and the large dynamic range combined with the cost-effectiveness of the electrochemical readout electronics could enable diagnostic tests at patients' homes for markers that are currently measured in centralized laboratories.

CRediT authorship contribution statement

Yves Blickenstorfer: Writing – original draft, Visualization, Software, Methodology, Investigation, Data curation, Conceptualization. **Vlastimil Jirasko:** Writing – original draft, Methodology, Investigation, Data curation. **Alexander Tanno:** Writing – review & editing, Methodology, Investigation, Funding acquisition, Conceptualization. **Sarah Dräger:** Writing – review & editing, Investigation, Conceptualization. **Darius Hoven:** Writing – review & editing, Software, Investigation. **Josephine Löhle:** Writing – review & editing, Investigation. **Stephan Leuch:** Writing – review & editing, Software, Investigation. **Yulya Mamedava:** Writing – review & editing, Investigation. **Sereina Livia Müller:** Writing – review & editing, Investigation. **Karoline Leuzinger:** Writing – review & editing, Investigation. **Michael Osthoff:** Supervision, Resources, Project administration, Methodology, Funding acquisition, Conceptualization. **János Vörös:** Writing – review & editing, Supervision, Project administration, Funding acquisition, Formal analysis, Conceptualization.

Declaration of competing interest

Data availability

Data will be made available on request.

Acknowledgement

Appendix A. Supplementary data

Supplementary data to this article can be found online at https://doi.org/10.1016/j.bios.2024.116524.

References

Ayranci, E., Duman, O., 2004. Binding of fluoride, bromide and iodide to bovine serum albumin, studied with ion-selective electrodes. Food Chem. 84, 539–543.

Blanco, I., Violán, C., Suñer, C., Garcia-Prieto, J., Argerich, M.J., Rodriguez-Illana, M., Moreno, N., Cardona, P.J., Blanco, A., Torán-Monserrat, P., Clotet, B., Bonet, J.M., Prat, N., 2022. Comparison between mid-nasal swabs and buccal swabs for SARS-CoV-2 detection in mild COVID-19 patients. J. Infect. 84, e78–e79.

Bourassa, L., Perchetti, G.A., Phung, Q., Lin, M.J., Mills, M.G., Roychoudhury, P., Harmon, K.G., Reed, J.C., Greninger, A.L., 2021. A SARS-CoV-2 nucleocapsid variant that affects antigen test performance. J. Clin. Virol. 141, 104900.

Corman, V.M., Haage, V.C., Bleicker, T., Schmidt, M.L., Mühlemann, B., Zuchowski, M., Jo, W.K., Tscheak, P., Möncke-Buchner, E., Müller, M.A., Krumbholz, A., Drexler, J. F., Drosten, C., 2021. Comparison of seven commercial SARS-CoV-2 rapid point-of-care antigen tests: a single-centre laboratory evaluation study. Lancet Microbe 2, e311–e319.

Davis, A., Tran, T., 1991. Gold dissolution in iodide electrolytes. Hydrometallurgy 26, 163–177.

Dequaire, M., Degrand, C., Limoges, B., 2000. An electrochemical metalloimmunoassay based on a colloidal gold label. Anal. Chem. 72, 5521–5528.

Ge, X., Asiri, A.M., Du, D., Wen, W., Wang, S., Lin, Y., 2014. Nanomaterial-enhanced paper-based biosensors. Trends Anal. Chem. 58, 31–39.

Glišić, B., Rychlewska, U., Djuran, M.I., 2012. Reactions and structural characterization of gold(iii) complexes with amino acids, peptides and proteins. Dalton Trans. 41, 6887–6901.

Green, T.A., 2014. Gold etching for microfabrication. Gold Bull. 47, 205–216.

Greenwald, J.L., Burstein, G.R., Pincus, J., Branson, B., 2006. A rapid review of rapid HIV antibody tests. Curr. Infect. Dis. Rep. 8, 125–131.

Hogg, C., Boots, S., Howorth, D., Williams, C., Heginbothom, M., Salmon, J., Howe, R., 2023. Test performance of lateral flow rapid antigen tests for COVID-19 in Welsh adult care home staff using routine surveillance data. PLoS One 18, e0290406.

Hwu, S., Blickenstorfer, Y., Ihle, S.J., Garzuel, M., Forró, C., Schmidheini, L., Demkó, L., Vörös, J., 2020. Theoretical and experimental investigation of ligand-induced particle–particle interactions. J. Phys. Chem. C 124, 1566–1574.

Ivandini, T.A., Wicaksono, W.P., Saepudin, E., Rismetov, B., Einaga, Y., 2015. Anodic stripping voltammetry of gold nanoparticles at boron-doped diamond electrodes and its application in immunochromatographic strip tests. Talanta 134, 136–143.

Khalid, M.F., Selvam, K., Jeffry, A.J.N., Salmi, M.F., Najib, M.A., Norhayati, M.N., Aziah, I., 2022. Performance of rapid antigen tests for COVID-19 diagnosis: a systematic review and Meta-Analysis. Diagnostics 12.

Leber, W., Lammel, O., Siebenhofer, A., Redlberger-Fritz, M., Panovska-Griffiths, J., Czypionka, T., 2021. Comparing the diagnostic accuracy of point-of-care lateral flow antigen testing for SARS-CoV-2 with RT-PCR in primary care (REAP-2). EClinicalMedicine 38, 101011.

Leuzinger, K., Gosert, R., Søgaard, K.K., Naegele, K., Bielicki, J., Roloff, T., Bingisser, R., Nickel, C.H., Khanna, N., Sutter, S.T., Widmer, A.F., Rentsch, K., Pargger, H., Siegemund, M., Stolz, D., Tamm, M., Bassetti, S., Osthoff, M., Battegay, M., Egli, A., Hirsch, H.H., 2021. Epidemiology and precision of SARS-CoV-2 detection following lockdown and relaxation measures. J. Med. Virol. 93, 2374–2384.

Liu, B., Du, D., Hua, X., Yu, X.Y., Lin, Y., 2014. Paper-based electrochemical biosensors: from test strips to paper-based microfluidics. Electroanalysis 26, 1214–1223.

Liu, G., Lin, Y.Y., Wang, J., Wu, H., Wai, C.M., Lin, Y., 2007. Disposable electrochemical immunosensor diagnosis device based on nanoparticle probe and immunochromatographic strip. Anal. Chem. 79, 7644–7653.

Liu, G., Wang, J., Barry, R., Petersen, C., Timchalk, C., Gassman, P.L., Lin, Y., 2008. Nanoparticle-based electrochemical immunosensor for the detection of phosphorylated acetylcholinesterase: an exposure biomarker of organophosphate pesticides and nerve agents. Chemistry 14, 9951–9959.

Liu, L., Meyers, K., Purpura, L.J., Nguyen, N., Mohri, H., Chang, J.Y., Annavajhala, M.K., Lopez, L., Lee, S.W., Shah, J., Lane, B., Cantos, A., Tukuru, S.A., Guo, Y., Ford, K., Chiu, Y.T., Sheng, Z., Choesang, T., Castor, D., Wang, M., Pili, C., Van Hoy, M.N., Wallach, A., Horton, J., Chen, Z., Rosenthal, S., McLaren, S., Jiang, B., Wang, F., Lu, H.H., Uhlemann, A.C., Ho, D.D., Yin, M.T., 2022. Development and performance of a point-of-care rapid antigen test for detection of SARS-COV-2 variants. J. Clin. Virol. 2, 100080.

Lu, F., Wang, K.H., Lin, Y., 2005. Rapid, quantitative and sensitive immunochromatographic assay based on stripping voltammetric detection of a metal ion label. Analyst 130, 1513–1517.

Mak, W.C., Beni, V., Turner, A.P.F., 2016. Lateral-flow technology: from visual to instrumental. Trends Anal. Chem. 79, 297–305.

Mao, X., Baloda, M., Gurung, A.S., Lin, Y., Liu, G., 2008. Multiplex electrochemical immunoassay using gold nanoparticle probes and immunochromatographic strips. Electrochem. Commun. 10, 1636–1640.

Mazurkiewicz, W., Podrażka, M., Jarosińska, E., Kappalakandy Valapil, K., Wiloch, M., Jönsson-Niedziółka, M., Witkowska Nery, E., 2020. Paper-based electrochemical sensors and how to make them (work). Chemelectrochem 7, 2939–2956.

Miočević, O., Cole, C.R., Laughlin, M.J., Buck, R.L., Slowey, P.D., Shirtcliff, E.A., 2017. Quantitative lateral flow assays for salivary biomarker assessment: a review. Front. Public Health 5, 133.

Mudanyali, O., Dimitrov, S., Sikora, U., Padmanabhan, S., Navruz, I., Ozcan, A., 2012. Integrated rapid-diagnostic-test reader platform on a cellphone. Lab Chip 12, 2678–2686.

Nian, H., Wang, J., Wu, H., Lo, J.G., Chiu, K.H., Pounds, J.G., Lin, Y., 2012. Electrochemical immunoassay of cotinine in serum based on nanoparticle probe and immunochromatographic strip. Anal. Chim. Acta 713, 50–55.

Nie, Z., Deiss, F., Liu, X., Akbulut, O., Whitesides, G.M., 2010. Integration of paper-based microfluidic devices with commercial electrochemical readers. Lab Chip 10, 3163–3169.

Peaper, D.R., Landry, M.L., 2014. Rapid diagnosis of influenza: state of the art. Clin. Lab. Med. 34, 365–385.

Puhach, O., Meyer, B., Eckerle, I., 2023. SARS-CoV-2 viral load and shedding kinetics. Nat. Rev. Microbiol. 21, 147–161.

Qi, P.H., Hiskey, J.B., 1993. Electrochemical behavior of gold in iodide solutions. Hydrometallurgy 32, 161–179.

Quesada-González, D., Merkoçi, A., 2015. Nanoparticle-based lateral flow biosensors. Biosens. Bioelectron. 73, 47–63.

Ramachandran, L.K., 1956. Protein-Iodine interaction. Chem. Rev. 56, 199–218.

Robinson, J.E., Wakelin, M., Ellis, J.E., 2007. Increased pregnancy rate with use of the clearblue easy fertility monitor. Fertil. Steril. 87, 329–334.

Schindelin, J., Arganda-Carreras, I., Frise, E., Kaynig, V., Longair, M., Pietzsch, T., Preibisch, S., Rueden, C., Saalfeld, S., Schmid, B., Tinevez, J.Y., White, D.J., Hartenstein, V., Eliceiri, K., Tomancak, P., Cardona, A., 2012. Fiji: an open-source platform for biological-image analysis. Nat. Methods 9, 676–682.

Szekely, J., Mongkolprasert, J., Jeayodae, N., Senorit, C., Chaimuti, P., Swangphon, P., Nanakorn, N., Nualnoi, T., Wongwitwichot, P., Pengsakul, T., 2022. Development, analytical, and clinical evaluation of rapid immunochromatographic antigen test for SARS-CoV-2 variants detection. Diagnostics 12.

Urusov, A.E., Zherdev, A.V., Dzantiev, B.B., 2019. Towards lateral flow quantitative assays: detection approaches. Biosensors 9.

Vashist, S.K., Schneider, E.M., Luong, J.H.T., 2014. Commercial Smartphone-Based devices and smart applications for personalized healthcare monitoring and management. Diagnostics 4, 104–128.

Wang, J., Xu, D., Kawde, A.N., Polsky, R., 2001. Metal nanoparticle-based electrochemical stripping potentiometric detection of DNA hybridization. Anal. Chem. 73, 5576–5581.

Wong, R., Tse, H. (Eds.), 2009. Lateral Flow Immunoassay. Humana Press.

Yetisen, A.K., Akram, M.S., Lowe, C.R., 2013. Paper-based microfluidic point-of-care diagnostic devices. Lab Chip 13, 2210–2251.